Transp Porous Med (2007) 70:213–229
DOI 10.1007/s11242-006-9096-x

ORIGINAL PAPER

Upscaling Forchheimer law

Jean-Louis Auriault · Christian Geindreau · Laurent Orgéas

Received: 9 March 2006 / Accepted: 15 December 2006 / Published online: 1 February 2007

Abstract We investigate the high velocity flow in heterogeneous porous media. The model is obtained by upscaling the flow at the heterogeneity scale where the Forchheimer law is assumed to be valid. We use the method of multiple scale expansions, which gives rigorously the macroscopic behaviour without any prerequisite on the form of the macroscopic equations. We show that Forchheimer law does not generally survive upscaling. The macroscopic flow law is strongly non-linear and anisotropic. A 2-point Padé approximation of the flow law in the form of a Forchheimer law is given. However, this approximation is generally poor. These results are illustrated in two particular cases: a layered composite porous media and a composite constituted by a square array of circular porous inclusions embedded in a porous matrix. We show that non-linearities are sources of anisotropy.

Keywords Flow in porous media · High velocity flow · Forchheimer law · Heterogeneous porous media · Upscaling

Nomenclature

Roman letters

$\mathbf{G}$	Macroscopic gradient of pressure
K	Permeability
K^{F}	Forchheimer equivalent permeability
K^{eff}	Effective permeability
l	Characteristic size of the pores
L	Macroscopic characteristic length
n	Medium 1 volume fraction
$\mathbf{n}$	Unit normal vector to Γ
p	Pressure

J.-L. Auriault · C. Geindreau (✉) · L. Orgéas
Laboratoire Sols Solides Structures (3S), UJF, INPG, CNRS, Domaine Universitaire, BP 53, 38041 Grenoble Cedex, France
e-mail: Christian.Geindreau@hmg.inpg.fr

$\mathcal{R}$	Dimensionless numbers
$\mathbf{v}$	Fluid velocity
V	Periodic cell
V_1, V_2	Medium 1 and 2 volumes in the periodic cell
$\mathbf{x}$	Dimensionless macroscopic space variable
$\mathbf{X}$	Dimensional space variable
$\mathbf{y}$	Dimensionless microscopic space variable
Greek letters	
β	Inertial coefficient
β^{eff}	Effective inertial coefficient
ε	Small parameter of separation of scale
Γ	Media 1 and 2 interface
ψ	Potential
μ	Viscosity
ρ	Fluid density

1 Introduction

The aim of this paper is to investigate the high velocity macroscopic flow law in a composite porous medium when assuming the validity of Forchheimer law at the component scale. Forchheimer law (Forchheimer 1901) is an empirical law for high permanent flow in porous media which simplicity makes it widely used at different scales in petroleum engineering (Skjetne and Auriault 1999). Its isotropic form writes

$$-\mathbf{G} = \left(\frac{\mu}{K} + \beta\rho|\mathbf{v}|\right)\mathbf{v}, \qquad |\mathbf{v}| = \sqrt{\mathbf{v}\cdot\mathbf{v}}, \tag{1}$$

where $\mathbf{G} = \nabla_X p$ is the gradient of pressure p with respect to the space variable $\mathbf{X}$, μ the viscosity, K the permeability, $\beta > 0$ an inertial coefficient, ρ the fluid density and $\mathbf{v}$ the fluid velocity. For anisotropic media, Forchheimer law can be generalized into

$$-\mathbf{G} = \mu\,\mathbf{K}^{-1}\mathbf{v} + \mathbf{H}(\mathbf{v}), \tag{2}$$

where $\mathbf{K}$ is the anisotropic permeability tensor and $\mathbf{H}$ is an homogeneous vectorial function of degree 2 of $\mathbf{v}$. As the velocity $\mathbf{v}$ goes to zero, Darcy law is recovered, so that Forchheimer law is often considered as valid whatever be $\mathbf{v}$. However, although it often represents an acceptable approximation, it has been demonstrated that at low velocity the departure from Darcy law is in $|\mathbf{v}|^3$ (Wodie and Levy 1991; Mei and Auriault 1991; Firdaous et al. 1997). More recently, the macroscopic behaviour of high velocity flow in porous media was rigorously investigated by Marušić-Paloka and Mikelić (2000), by upscaling Navier–Stokes equations at the pore scale. They clearly show that in general, Forchheimer law is not strictly verified. However, in Fourar et al. (2004) it is shown from numerical experiments that 3-D flow are "correctly" modeled by Forchheimer equation. Finally, let us remark that turbulent flow in simple and complex media is usually described by a modified Forchheimer equation [see Skjetne and Auriault (1999) and references herein].

In this paper, we investigate the macroscopic flow law in a composite porous medium from low to high velocity by rigorously upscaling Forchheimer equation at the component scale. A similar study was conducted by numerical way by Fourar

et al. (2005), under some restrictive conditions: Forchheimer law is assumed as valid at the macro-scale, $b = \beta\sqrt{K}$ is kept constant in the composite medium and the local Forchheimer equation is linearized by considering the Reynolds number as a constant over each constituent.

To obtain the macroscopic flow model from the component scale description, we use an upscaling technique, i.e. the method of multiple scale expansions. Heterogeneous systems as for example porous media may be modelled by an equivalent macroscopic continuous system if the condition of separation of scales is verified (Bensoussan et al. 1978; Sanchez-Palencia 1980)

$$\varepsilon = \frac{l}{L} \ll 1, \tag{3}$$

where l and L are the characteristic lengths of the heterogeneities and of the macroscopic sample or excitation, respectively. The macroscopic equivalent model is obtained from the description at the heterogeneity scale by (Auriault 1991): (i) assuming the medium to be periodic, without loss of generality. It is clear that real porous media are rarely periodic. However, when the condition of separation of scales is fulfilled, the structure of the macroscopic description of periodic and random media are similar. Finally, notice that the periodic boundary conditions are widely used to compute the effective properties of random media (Kanit et al. 2003, 2006); (ii) writing the local description in a dimensionless form; (iii) evaluating the dimensionless numbers with respect to the scale ratio ε; (iv) looking for the unknown fields in the form of asymptotic expansions in powers of ε; (v) solving the successive boundary-value problems that are obtained after introducing these expansions in the local dimensionless description. The macroscopic equivalent model is obtained from compatibility conditions which are the necessary conditions for the existence of solutions to the boundary-value problems. The main advantages of the method rely upon the possibility of: (a) avoiding prerequisites at the macroscopic scale; (b) modelling finite size macroscopic samples; (c) modelling macroscopically non-homogeneous media or phenomena; (d) modelling problems with several separations of scales; (e) modelling several simultaneous phenomena; (f) determining whether the system "medium+ phenomena" is homogenisable or not; (g) providing the domains of validity of the macroscopic models.

In Sect. 2, we investigate the macroscopic flow model in the composite porous medium, by assuming Forchheimer law to be valid at the component scale. In general Forchheimer law does not survive upscaling. A 2-point Padé approximation of the macroscopic flow model is given in Sect. 3 from the behaviours at small and large gradients of pressure. This approximate model is in the form of a Forchheimer law. Analytical expressions of the macroscopic flow law are presented in the case of a layered composite porous media (Sect. 4), which permits to test the accuracy of the Padé approximation. Two examples are investigated for low and high contrast properties of the components. The relative error introduced by the Padé approximation is found to be less than 15%. Finally, Sect. 5 is devoted to the numerical study of a 2D composite constituted by a square array of circular porous inclusions in a porous matrix with different properties. The flow parallel to the axis of symmetry of the microstructure is first considered. The effective permeability of this composite is determined and compared to the Padé approximation. We show that the relative error introduced by the Padé approximation strongly depends on the volume fraction of both constituents and the contrast properties between the matrix and the inclusions. This error

may reach 80%. The flow out of the axis of symmetry of the microstructure is then considered. Our numerical results show that the macroscopic velocity is not aligned with the imposed pressure gradient in the high pressure gradient range.

2 Derivation of the macroscopic flow law

The considered composite porous medium is spatially periodic and consists of repeated unit cells (parallelepipeds), see Fig. 1. For simplicity, we consider a two component porous composite. There are two characteristic length scales in this problem: the characteristic microscopic length scale l of the porous components and of the unit cell, and the macroscopic length scale L that may be represented by the macroscopic sample size or associated to the macroscopic flow. We assume that the two length scales l and L are well separated

$$\frac{l}{L} = \varepsilon \ll 1. \tag{4}$$

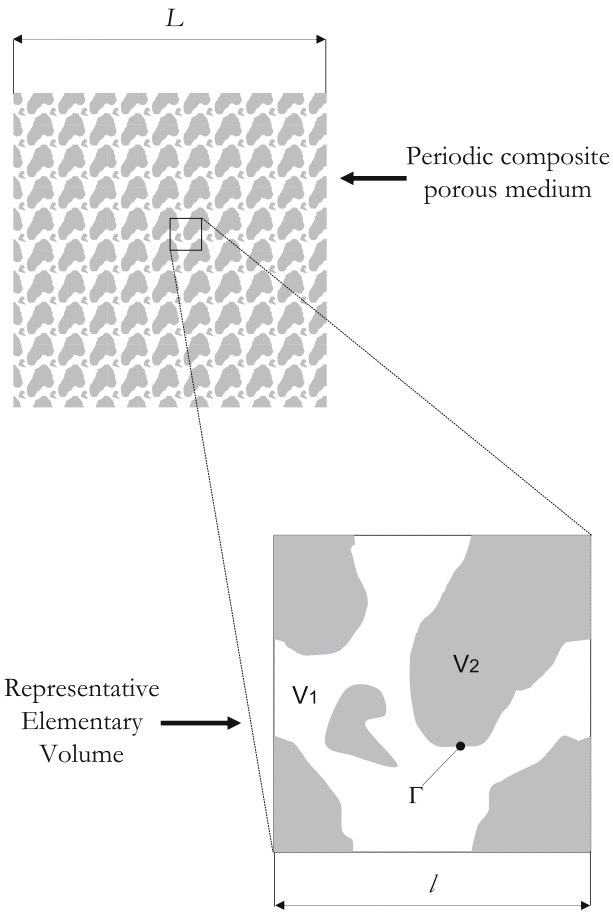

Fig. 1 A period of the porous medium

The unit cell is denoted by V and is bounded by ∂V, the two component parts of the unit cell are denoted by V_1 and V_2, respectively, and their interface inside the unit cell is Γ.

2.1 Local description

An incompressible newtonian fluid is filtrating at high velocity through the composite porous medium. We assume that the flow of this fluid in both constituents is described by the isotropic Forchheimer law (1)

$$-\mathbf{G} = \left(\frac{\mu}{K} + \beta\rho\,|\mathbf{v}|\right)\,\mathbf{v}, \qquad |\mathbf{v}| = \sqrt{\mathbf{v}\cdot\mathbf{v}}. \tag{5}$$

The local description is completed by the incompressibility condition

$$\nabla_X \cdot \mathbf{v} = 0, \tag{6}$$

and the continuity of the normal flux and of the pressure on Γ. It is convenient to rewrite (1) in a reverse form. From (1) we have

$$|\mathbf{G}| = \left(\frac{\mu}{K} + \beta\rho\,|\mathbf{v}|\right)\,|\mathbf{v}|, \tag{7}$$

which positive solution $|\mathbf{v}|$ is

$$|\mathbf{v}| = -\frac{1}{2\beta\rho}\left(-\frac{\mu}{K} + \sqrt{\frac{\mu^2}{K^2} + 4\beta\rho|\mathbf{G}|}\right). \tag{8}$$

Introducing this expression of $|\mathbf{v}|$ into (1) yields

$$\mathbf{v} = -\frac{K^{\mathrm{F}}}{\mu}\mathbf{G}, \qquad K^{\mathrm{F}} = \frac{2K}{1+\sqrt{1+\dfrac{4\beta\rho K^2}{\mu^2}|\mathbf{G}|}} \tag{9}$$

where K^{F} is a Forchheimer permeability. Finally, the flow is described by

$$\nabla_X \cdot \left(\frac{K^{\mathrm{F}}}{\mu}\mathbf{G}\right) = 0. \tag{10}$$

2.2 Dimensionless local description

All physical quantities are made dimensionless, $\phi = \phi_c\phi^*$, where ϕ_c is a characteristic value of the physical variable ϕ and ϕ^* is dimensionless. The choice of ϕ_c implies $\phi^* = \mathcal{O}(1)$ which means $\varepsilon \ll \phi^* \ll \varepsilon^{-1}$. Due to the separation of scales, there are two characteristic values of the space variable, l and L. That introduces two dimensionless space variables, $\mathbf{y} = \mathbf{X}/l$ and $\mathbf{x} = \mathbf{X}/L = \varepsilon\mathbf{y}$, respectively. All quantities are functions of these two dimensionless variables.

We assume that the two terms in the right hand member of the Forchheimer equation (1) are of the same order of magnitude and we remark that the flow is caused by a macroscopic gradient of pressure, which is equilibrated by these two terms

$$\frac{p_c}{L} = \mathcal{O}\left(\frac{\mu_c v_c}{K_c}\right) = \mathcal{O}(\beta_c\rho_c v_c^2). \tag{11}$$

Other situations where one of the last two terms is smaller appear as particular cases of the investigated estimation (11), see part 3. When using l as the characteristic length, the dimensionless form of the local description (10) can be put in the form

$$\nabla_y \cdot \left(\frac{K^{\mathrm{F}*}}{\mu^*} \nabla_y p^* \right) = 0, \qquad K^{\mathrm{F}*} = \frac{2K^*}{1 + \sqrt{1 + \mathcal{R}\varepsilon^{-1} R^* |\nabla_y p^*|}}, \tag{12}$$

where $R^*(\mathbf{y}, \mathbf{x}) = 4\beta^* \rho^* K^{*2} / \mu^{*2}$ (here $\rho^* = 1$ and $\mu^* = 1$) is $\mathbf{y}$-periodic and possibly $\mathbf{x}$ dependent and the dimensionless number $\mathcal{R}$ can be evaluated by using relations (11)

$$\mathcal{R} = \frac{\beta_c \rho_c {K_c}^2}{{\mu_c}^2} \frac{p_c}{l} \frac{l}{L} = \mathcal{O}(1). \tag{13}$$

For simplicity we consider $\mathcal{R} = 1$ in the following case. On Γ we have the continuity of the pressure and of the normal flux

$$[p^*] = 0 \quad \text{on} \quad \Gamma, \tag{14}$$

$$[\mathbf{v}^*] \cdot \mathbf{n} = \left[-\frac{K^{\mathrm{F}*}}{\mu^*} \nabla_y p^* \right] . \mathbf{n} = 0 \quad \text{on} \quad \Gamma. \tag{15}$$

We will also need the dimensionless form of the Forchheimer law (1)

$$-\varepsilon^{-1} \nabla_y p^* = \left(\frac{\mu^*}{K^*} + \beta^* \rho^* \, |\mathbf{v}^*| \right) \mathbf{v}^*. \tag{16}$$

2.3 Upscaling

The pressure p^* and the velocity $\mathbf{v}^*$ are looked for in the form of the following asymptotic expansions

$$p^* = p^{*(0)}(\mathbf{x}, \mathbf{y}) + \varepsilon p^{*(1)}(\mathbf{x}, \mathbf{y}) + \varepsilon^2 p^{*(2)}(\mathbf{x}, \mathbf{y}) + \cdots, \tag{17}$$

$$\mathbf{v}^* = \mathbf{v}^{*(0)}(\mathbf{x}, \mathbf{y}) + \varepsilon \mathbf{v}^{*(1)}(\mathbf{x}, \mathbf{y}) + \varepsilon^2 \mathbf{v}^{*(2)}(\mathbf{x}, \mathbf{y}) + \cdots, \tag{18}$$

where the different terms $p^{*(i)}$ and $\mathbf{v}^{*(i)}$ in the asymptotic expansion are dimensionless and V-periodic in $\mathbf{y}$. Introducing these expansions into the dimensionless local description and extracting like power terms in ε yield different boundary value problems to be investigated.

At the order ε^{-1}, equation (16) gives

$$\nabla_y p^{*(0)} = \mathbf{0}, \qquad p^{*(0)} = p^{*(0)}(\mathbf{x}). \tag{19}$$

Let us now consider equation (12_1) at the order ε^0, together with the associated conditions on Γ

$$\nabla_y \cdot \left(\frac{K^{\mathrm{F}*(0)}}{\mu^*} (\nabla_y p^{*(1)} + \nabla_x p^{*(0)}) \right) = 0, \tag{20}$$

$$K^{\mathrm{F}*(0)} = \frac{2K^*}{1 + \sqrt{1 + R^* |\nabla_y p^{*(1)} + \nabla_x p^{*(0)}|}}, \tag{21}$$

where $p^{*(1)}$ is $\mathbf{y}$-periodic and continuous on Γ, as well as the normal flux,

$$[p^{*(1)}] = 0 \quad \text{on} \quad \Gamma, \tag{22}$$

$$[\mathbf{v}^{*(0)}] \cdot \mathbf{n} = \left[\frac{K^{\mathrm{F}*(0)}}{\mu^*} (\nabla_y p^{*(1)} + \nabla_x p^{*(0)}) \right] . \mathbf{n} = 0 \quad \text{on} \quad \Gamma. \tag{23}$$

To investigate this boundary value problem for $p^{*(1)}$, let us introduce the Hilbert space $\mathcal{V}$ of all $\mathbf{y}$-periodic functions, of zero average on V and continuous on Γ, with the scalar product

$$(p, q)_{\mathcal{V}} = \int_V \nabla_y p \cdot \nabla_y q \, \mathrm{d}V. \tag{24}$$

Multiplying (20) by a test function q of $\mathcal{V}$, and integrating by parts on V yields the weak formulation

$$\forall q \in \mathcal{V}, \quad \int_V \frac{K^{\mathrm{F}*(0)}}{\mu^*} (\nabla_y p^{*(1)} + \nabla_x p^{*(0)}) \cdot \nabla_y q \, \mathrm{d}V = 0. \tag{25}$$

To investigate this strongly non-linear formulation, we pose $(\nabla_y p^{*(1)} + \nabla_x p^{*(0)}) = \mathbf{Y}(p^{*(1)})$ and we note that the quantity $-\mathbf{v}^{*(0)} = K^{\mathrm{F}*(0)}(\mathbf{Y})\mathbf{Y}/\mu^*$ derives from a potential ψ

$$-\mathbf{v}^{*(0)} = \frac{K^{\mathrm{F}*(0)}(\mathbf{Y})}{\mu^*} \mathbf{Y} = \frac{\partial \psi}{\partial \mathbf{Y}}, \tag{26}$$

with

$$\psi = \frac{2}{3\mu^* R^{*2}} (1 + R^* |\mathbf{Y}|)(2(1 + R^* |\mathbf{Y}|)^{1/2} - 3). \tag{27}$$

Furthermore it is possible to show that ψ is convex

$$\forall p, q \in \mathcal{V}, \quad \psi(\mathbf{Y}(p)) - \psi(\mathbf{Y}(q)) - \frac{\partial \psi}{\partial \mathbf{Y}}(q) \cdot (\mathbf{Y}(p) - \mathbf{Y}(q)) \geq 0. \tag{28}$$

Formulation (25) can be rewritten in the form

$$\forall q \in \mathcal{V}, \quad \int_V \frac{\partial \psi}{\partial \mathbf{Y}} (p^{*(1)}) \cdot \nabla_y q \, \mathrm{d}V = 0, \tag{29}$$

which gives with $q = p^{*(1)}$

$$\int_V \frac{\partial \psi}{\partial \mathbf{Y}} (p^{*(1)}) \cdot \nabla_y p^{*(1)} \, \mathrm{d}V = 0. \tag{30}$$

Let now $q = p^{*(1)}$ in (28) and use (29) and (30). We are left with

$$\forall p \in \mathcal{V}, \quad \psi(\mathbf{Y}(p)) - \psi(\mathbf{Y}(p^{*(1)})) \geq 0. \tag{31}$$

The problem reduces to the minimization of the convex ψ. Therefore, there exists a unique $p^{*(1)}$ to formulation (25). Taking into account the zero volume average extraneous condition introduced to define space $\mathcal{V}$, yields the solution of the boundary value problem (20–21) in the form

$$p^{*(1)} = \mathcal{F}^*(\nabla_x p^{*(0)}) + \bar{p}^{*(1)}(\mathbf{x}), \tag{32}$$

where $\mathcal{F}^*$ is a non-linear functional. Finally, at the next order, equation (12_1) gives

$$\nabla_x \cdot \mathbf{v}^{*(0)} + \nabla_y \cdot \mathbf{v}^{*(1)} = 0, \qquad \mathbf{v}^{*(0)} = -\frac{K^{F*(0)}}{\mu^*}(\nabla_y p^{*(1)} + \nabla_x p^{*(0)}), \tag{33}$$

where $\mathbf{v}^{*(1)}$ is a periodic vector. Volume averaging this last equation (a necessary and sufficient condition for the existence of $\mathbf{v}^{*(1)}$) yields the first order approximation of the macroscopic flow description

$$\nabla_x \cdot \langle \mathbf{v}^{*(0)} \rangle = 0, \qquad \langle \mathbf{v}^{*(0)} \rangle = \frac{1}{V}\int_V \mathbf{v}^{*(0)}\, \mathrm{d}V = -\mathcal{G}^*(\nabla_x p^{*(0)}), \tag{34}$$

where the $\mathcal{G}_i^*$'s are non-linear functionals.
Returning to physical quantities, the macroscopic description becomes

$$\nabla_X \cdot \langle \mathbf{v} \rangle = \mathcal{O}(\varepsilon \nabla_X \cdot \langle \mathbf{v} \rangle), \qquad \langle \mathbf{v} \rangle = -\mathcal{G}(\nabla_X p) + \mathcal{O}(\varepsilon \langle \mathbf{v} \rangle). \tag{35}$$

In general, the macroscopic flow law (34_2) cannot be put in the form of a Forchheimer law. Therefore, Forchheimer law generally not survives upscaling. In the next section, we look for a Padé approximation of the macroscopic flow law in the form of a Forchheimer law.

3 Padé–Forchheimer approximation of the macroscopic flow law

For practical interest, it may be useful to look for a simple form of the macroscopic flow law, such as those using Padé approximants. For that purpose, first we investigate the low and high velocity regimes.
For small gradients of pressure, Forchheimer laws (1) and (9) reduce to Darcy law

$$\mathbf{v} = -\frac{K}{\mu}\mathbf{G}_{\text{small}}, \qquad -\mathbf{G}_{\text{small}} = \frac{\mu}{K}\,\mathbf{v}. \tag{36}$$

It is well-known (see, e.g., Sanchez-Palencia 1980; Mei and Auriault 1989) that the corresponding macroscopic flow law is a Darcy law with an effective permeability tensor $\mathbf{K}^{\text{eff}}$ (for simplicity we drop the ε order term)

$$\nabla_X \cdot \langle \mathbf{v} \rangle = 0, \qquad -(\nabla_X p)_{\text{small}} = \mu\, (\mathbf{K}^{\text{eff}})^{-1} \langle \mathbf{v} \rangle. \tag{37}$$

For large velocities, Forchheimer law reduces to Chézy law. Equations (1) and (9) become, respectively

$$-\mathbf{G}_{\text{large}} = \beta\rho\, |\mathbf{v}|\, \mathbf{v}, \quad \mathbf{v} = -\frac{K^{\text{F}}}{\mu}\mathbf{G}_{\text{large}}, \tag{38}$$

$$K^{\text{F}} = \frac{\mu}{\sqrt{\beta\rho\, |\mathbf{G}_{\text{large}}|}}. \tag{39}$$

The upscaling is as above. By neglecting again the ε order error we have as in Sect. 2.3

$$\begin{aligned} \nabla_X \cdot \langle \mathbf{v} \rangle = 0, \quad \langle \mathbf{v} \rangle &= -\mathcal{H}((\nabla_X p)_{\text{large}}), \\ -(\nabla_X p)_{\text{large}} &= \mathcal{H}^{-1}(\langle \mathbf{v} \rangle), \end{aligned} \tag{40}$$

where $\mathcal{G}$ tends to $\mathcal{H}$ for large velocity. However now, due to the particular form of the local Forchheimer law (38), $\nabla_y p^{*(1)}$ is an homogeneous function of degree 1 and $\mathbf{v}^{*(0)}$ an homogeneous function of degree 1/2 of $\nabla_x p^{*(0)}$. Therefore, in (40) $(\nabla_X p)_{\text{large}}$ is an homogeneous vectorial function of degree 2 of $\langle \mathbf{v} \rangle$.
From the lower and the upper limits (37) and (40) of the macroscopic flow law, respectively, a 2-point Padé approximation is easily constructed

$$-\nabla_X p = \mu\, (\mathbf{K}^{\text{eff}})^{-1} \langle \mathbf{v} \rangle + \mathcal{H}^{-1}(\langle \mathbf{v} \rangle). \tag{41}$$

Equation (41) stands for an anisotropic Forchheimer law.

4 Layered composite porous media

To check the accuracy of (41), we first consider the laminated composite porous medium shown in Fig. 2. Both components 1 and 2 are homogeneous. We successively address the 1-D macroscopic flow perpendicular and parallel to the layer direction. This very simple geometry can be investigated directly from the local description (5–10), without using the homogenization formalism.

4.1 Flow perpendicular to the layers

In this case the velocity is in the X_2 direction and, due to the incompressibility condition $\partial v_2 / \partial X_2 = 0$, it is a constant in the composite medium. Therefore the macroscopic flow is directly obtained by averaging the local Forchheimer law (1) with respect to space variable X_2, which at the first order of approximation gives (at this order, pressure p is a constant in the period)

$$-\frac{\partial p}{\partial X_2} = \left(\mu \left\langle \frac{1}{K} \right\rangle + \langle \beta \rangle \rho\, |v_2| \right) v_2, \tag{42}$$

where $\left\langle \frac{1}{K} \right\rangle^{-1}$ is the effective permeability K^{eff} and $\langle \beta \rangle = n\beta_1 + (1-n)\beta_2 = \beta^{\text{eff}}$ is the effective inertial coefficient in the direction perpendicular to the layers. In this particular case, the macroscopic flow follows a Forchheimer law (42), which is identical with the Padé approximation (41).

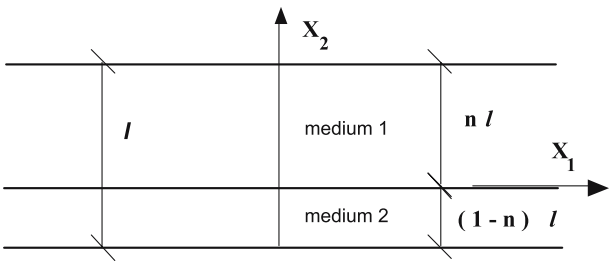

Fig. 2 A period of the layered porous medium

4.2 Flow parallel to the layers

The fluid flow is now in direction X_1. It is easy to check that the pressure in the period is independent of X_2. Therefore, the macroscopic flow is directly obtained by averaging Forchheimer law with respect to space variable X_2 in its form (9)

$$\langle v_1\rangle = -\frac{\langle K^{\mathrm{F}}\rangle}{\mu}\,\frac{\partial p}{\partial X_1}, \qquad \langle K^{\mathrm{F}}\rangle = \left\langle \frac{2K}{1+\sqrt{1+\dfrac{4\beta\rho K^2}{\mu^2}\left|\dfrac{\partial p}{\partial X_1}\right|}}\right\rangle. \tag{43}$$

Obviously (43_1) is not a Forchheimer law, whereas the Padé approximation (41) writes

$$-\frac{\partial p}{\partial X_1} = \frac{\mu}{\langle K\rangle}\langle v_1\rangle_{\text{Padé}} + \left(\left\langle\frac{1}{\sqrt{\beta}}\right\rangle\right)^{-2}\rho\,|\langle v_1\rangle_{\text{Padé}}|\langle v_1\rangle_{\text{Padé}}, \tag{44}$$

which is a Forchheimer law with $K^{\text{eff}} = \langle K\rangle$ and $\beta^{\text{eff}} = \left\langle\dfrac{1}{\sqrt{\beta}}\right\rangle^{-2}$. By construction, both flow laws (43) and (44) coincide for small and large velocities, respectively.

To investigate the accuracy of the Padé approximation, we have plotted in Fig. 3 the relative error $(\langle v_1\rangle_{\text{Padé}} - \langle v_1\rangle)/\langle v_1\rangle$ versus dimensionless gradient of pressure $G^* = (4\beta^{\text{eff}}\rho(K^{\text{eff}})^2/\mu^2)\frac{\partial p}{\partial X_1}$ for two composite materials which volume fractions of each constituent is $f = 0.5$: a gravel–sand composite with high contrast properties, $K_1 = 3.76\times10^{-8}$ m^2, $\beta_1 = 1.3\times10^{3}$ m^{-1} for the gravel, $K_2 = 3\times10^{-10}$ m^2, $\beta_2 = 25\times10^{3}$ m^{-1} for the sand, data from Venkataraman and Rama Mohan Rao (1998), and a geosynthetic composite with small contrast properties, $K_1 = 4.15\times10^{-7}$ m^2, $\beta_1 = 64.6$ m^{-1}, $K_2 = 3.3\times10^{-8}$ m^2, $\beta_2 = 314$ m^{-1}, data from Bordier and Zimmer (2000). In these two examples, we see that the relative velocity error does not exceed 15%. However, the accuracy of the Padé approximation remains poorer for the high contrast gravel–sand composite in a larger range of the gradient of pressure.

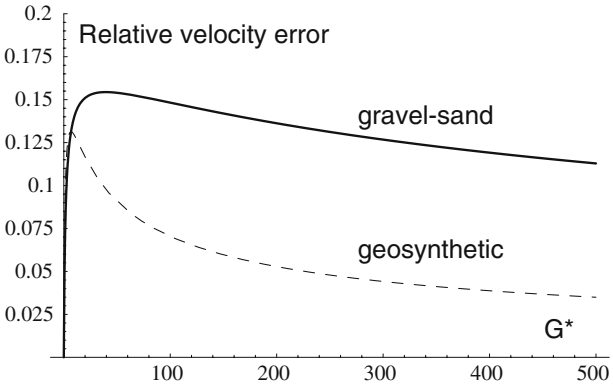

Fig. 3 Relative velocity error introduced by the Padé approximation versus the gradient of pressure. Bold: gravel–sand composite; dashed: geosynthetic composite

5 Composite constituted by a square array of circular porous inclusions embedded in a porous matrix

5.1 Microstructure

We consider now a composite constituted by a square array of circular porous inclusions (volume fraction f) embedded in a porous matrix (Fig. 4). Due to the symmetries of the REV which shows tetratropy, the linear Darcy regime is isotropic, $\mathbf{K}^{\text{eff}} = K^{\text{eff}}\,\mathbf{I}$. As previously, a gravel–sand composite with high contrast properties is considered: $K_1 = 3.76 \times 10^{-8}\ \text{m}^2$, $\beta_1 = 1.3 \times 10^3\ \text{m}^{-1}$ and $K_2 = 3 \times 10^{-10}\ \text{m}^2$, $\beta_2 = 25 \times 10^3\ \text{m}^{-1}$ for the gravel and the sand, respectively. In the following, two cases are investigated:

- Case 1: inclusions of sand are embedded in a matrix of gravel,
- Case 2: inclusions of gravel are embedded in a matrix of sand.

5.2 Numerical procedure

In order to study the macroscopic flow law, we first investigate the following well-posed boundary values problem (20–21) for $p^{*(1)} \in \mathcal{V}$ in its dimensional form :

$$\nabla_X \cdot \left(\frac{K^{\text{F}(0)}}{\mu} (\nabla_X(\varepsilon p^{(1)}) + \nabla_X p^{(0)}) \right) = 0 \quad \text{in} \quad V = V_1 \cup V_2, \tag{45}$$

$$\left[\frac{K^{\text{F}(0)}}{\mu} (\nabla_X(\varepsilon p^{(1)}) + \nabla_X p^{(0)}) \right] .\mathbf{n} = 0 \quad \text{on} \quad \Gamma, \tag{46}$$

with

$$K^{\text{F}(0)} = \frac{2K}{1 + \sqrt{1 + \dfrac{4\rho\beta K^2}{\mu^2} |\nabla_X(\varepsilon p^{(1)}) + \nabla_X p^{(0)}|}}, \tag{47}$$

where the macroscopic pressure gradient $\mathbf{G} = \nabla_X p^{(0)}$ is given on the entire REV. This boundary values problem was solved using the finite element method (Femlab 2005)

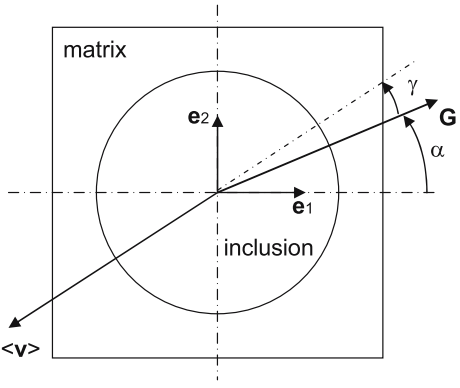

Fig. 4 Square array of circular inclusions embedded in a matrix. Representative Elementary Volume (REV)

with triangular mesh and quadratic polynomial interpolation. Hence, the microstructure is submitted to a macroscopic pressure gradient $\mathbf{G} = \nabla_X p^{(0)}$ of intensity denoted $|G|$ such that (see Fig. 4)

$$\mathbf{G} = \nabla_X p^{(0)} = |G|(\cos\alpha \mathbf{e}_1 + \sin\alpha \mathbf{e}_2), \tag{48}$$

where $\alpha = (\widehat{\mathbf{e}_1, \mathbf{G}})$. The resulting macroscopic velocity $\langle \mathbf{v} \rangle = \langle \mathbf{v}^{(0)} \rangle$ of intensity $|\langle v \rangle|$ is such that

$$\langle \mathbf{v} \rangle = \langle \mathbf{v}^{(0)} \rangle = -|\langle v \rangle|(\cos(\alpha + \gamma)\mathbf{e}_1 + \sin(\alpha + \gamma)\mathbf{e}_2) \tag{49}$$

where $\gamma = (\widehat{\mathbf{G}, -\langle \mathbf{v} \rangle})$ (see Fig. 4).

5.3 Numerical results: on axis-flow

We first impose a macroscopic gradient of pressure $\mathbf{G} = |G|\mathbf{e}_1$ ($\alpha = 0$). Due to the symmetry of the microstructure $\langle \mathbf{v} \rangle = -|\langle v \rangle|\mathbf{e}_1$ ($\gamma = 0$). The apparent permeability of the composite along $\mathbf{e}_1$-axis is defined as,

$$K^{\text{app}}(|G|) = \frac{\mu |\langle v \rangle|}{|G|}. \tag{50}$$

Figures 5 and 6 present the evolution of the apparent permeability $K^{\text{app}}(G)$ versus the macroscopic gradient of pressure G for different volume fractions of inclusion f in the case 1 and 2, respectively. Evolutions of the Forchheimer equivalent permeability K^{F} of each constituent are also presented on theses figures. On both figures, we observe that the apparent permeability $K^{\text{app}}(|G|)$ decreases with increasing the macroscopic gradient of pressure $|G|$, just as Forchheimer permeability K^{F} does. However, relation (50) is not a Forchheimer law. Let us compare it to the Padé–Forchheimer approximation (41). This one is written,

$$-|G|\mathbf{e}_1 = -\left(\frac{\mu}{K^{\text{eff}}} + \beta^{\text{eff}} \rho\, |\langle v \rangle|\right) |\langle v \rangle| \mathbf{e}_1, \tag{51}$$

where K^{eff} and β^{eff} for both cases investigated are summarized in Table 1. From relation (51), we can defined the Padé equivalent permeability,

$$K_{\text{Pade}}(|G|) = \frac{2K^{\text{eff}}}{1 + \sqrt{1 + \dfrac{4\rho\beta^{\text{eff}} K^2}{\mu^2}|G|}}. \tag{52}$$

As previously, to investigate the accuracy of the Padé approximation, we have plotted in Figs. 7, 8 the relative error $(K_{\text{Pade}} - K^{\text{app}})/K^{\text{app}}$ versus gradient of pressure $|G|$. By construction, both flow laws (50) and (51) coincide for small and large gradient of pressure, respectively. Therefore, in cases 1 and 2, the relative error is obviously negligible for small and large gradient of pressure. For intermediate values of pressure gradient, the relative error increases with increasing the volume fraction of inclusion. It also depends on the properties of the matrix and the inclusion. In the case 1, the relative error (Fig. 7) is more than 80% for volume fractions of inclusion larger than 0.7. In the case 2 (Fig. 8), the relative error is lower than 5% for volume fractions of inclusion less than 0.7.

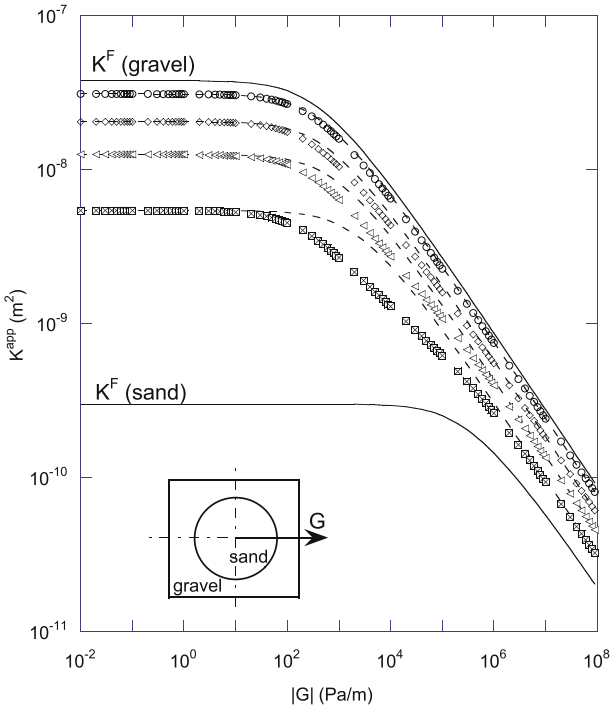

Fig. 5 Case 1: inclusions of sand embedded in a matrix of gravel. Evolution of the apparent permeability K^{app} of the composite medium versus the gradient of pressure $|G|$ for different volume fraction of inclusion. ($\circ$) $f = 0.1$, ($\diamond$)$f = 0.3$, ($\triangleleft$) $f = 0.5$, ($\boxtimes$) $f = 0.7$. Dashed lines represent Padé–Forchheimer approximations given by equation (52). Continuous lines represent the evolution of the Forchheimer equivalent permeability K^{F} of both constituents

5.4 Numerical results: off axis-flow

In the previous section, we have shown that the macroscopic flow law of such composite is not a Forchheimer law. The aim of this last section is to show that non-linearities introduce anisotropy in the macroscopic flow. For that purpose, we now suppose for example that the macroscopic gradient of pressure is $\mathbf{G} = |G|(\sqrt{3}/2\mathbf{e}_1 + 1/2\ \mathbf{e}_2)$, i.e. $\alpha = \pi/6$ in equation (48).

Figure 9 shows the evolution of the angle $\gamma = (\widehat{\mathbf{G}, -\langle\mathbf{v}\rangle})$ (see Fig. 4) versus the pressure gradient $|G|$ for different volume fractions of inclusion in the case 1. Obviously, the angle γ equals zero for small value of the pressure gradient ($|G| < 0.1$), i.e. when inertial effects are negligible at the local scale in both the matrix and the inclusion. For pressure gradient larger than 0.1, the evolution of γ versus the pressure gradient is complex and depends on the volume fraction of inclusion.

Figure 10 shows the evolution of the ratio $|\langle\mathbf{v}\rangle|/(|\langle\mathbf{v}_1\rangle + \langle\mathbf{v}_2\rangle|)$ versus the pressure gradient $|G|$ for different volume fractions of inclusion in the case 1. Velocities $\langle\mathbf{v}\rangle$, $\langle\mathbf{v}_1\rangle$ and $\langle\mathbf{v}_2\rangle$ are the macroscopic velocities when the composite is submitted to different macroscopic pressure gradient $|G|(\sqrt{3}/2\ \mathbf{e}_1 + 1/2\ \mathbf{e}_2)$, $|G|\sqrt{3}/2\ \mathbf{e}_1$ and $|G|\ 1/2\ \mathbf{e}_2$, respectively. Figure 10 shows that this ratio is equal to one for small value of the pressure gradient ($|G| < 0.1$), i.e. when inertial effects are negligible at the local scale

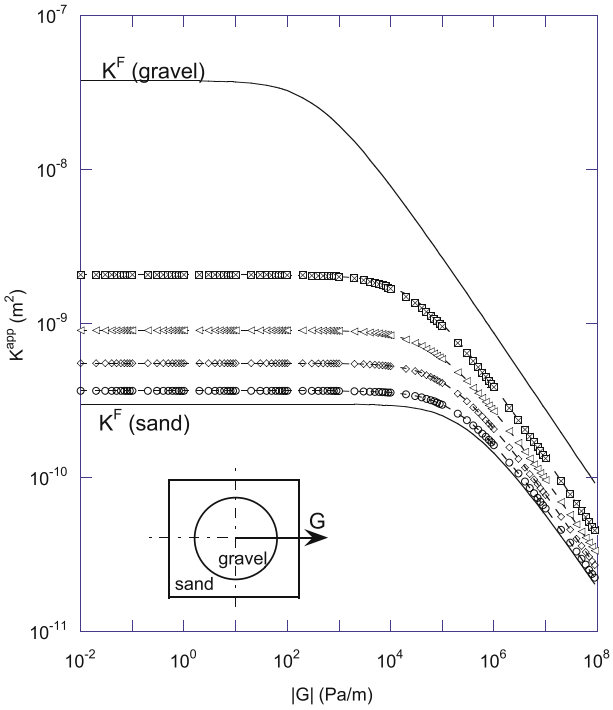

Fig. 6 Case 2: inclusions of gravel embedded in a matrix of sand. Evolution of the apparent permeability K^{app} of the composite medium versus the gradient of pressure $|G|$ for different volume fractions of inclusion. (○) $f = 0.1$, (◇)$f = 0.3$, (◁) $f = 0.5$, (☒) $f = 0.7$. Dashed lines represent Padé–Forchheimer approximations given by equation (52). Continuous lines represent the evolution of the Forchheimer equivalent permeability K^{F} of both constituents

Table 1 Case 1 and 2: values of K^{eff} and β^{eff} for different volume fractions of inclusion f

f [−]	K^{eff}—Case 1 [m^2]	β^{eff}—Case 1 [m^{-1}]	K^{eff}—Case 2 [m^2]	β^{eff}—Case 2 [m^{-1}]
0.1	3.09E-08	1.70E+03	3.66E-10	2.09E+04
0.3	2.04E-08	2.93E+03	5.52E-10	1.44E+04
0.5	1.25E-08	5.20E+03	9.03E-10	9.51E+03
0.7	5.41E-09	1.02E+04	2.07E-09	5.25E+03

in both the matrix and the inclusion. As previously, for pressure gradient larger than 0.1, the evolution of this ratio versus the pressure gradient is complex and depends on the volume fraction of inclusion.

Results presented in Figs. 9, 10 show that $\gamma = 0$ and $|\langle \mathbf{v} \rangle|/(|\langle \mathbf{v}_1 \rangle + \langle \mathbf{v}_2 \rangle|) = 1$ when the pressure gradient is small ($|G| < 0.1$). This is the direct consequence of both the linearity of the flow behaviour in this regime and the tetratropy of the microstructure which yields an isotropic macroscopic flow law. When $|G| > 0.1$, inertial effects in the matrix or/and in the inclusion are not negligible. Figures 9 and 10 show that $\gamma \neq 0$ and $|\langle \mathbf{v} \rangle|/(|\langle \mathbf{v}_1 \rangle + \langle \mathbf{v}_2 \rangle|) \neq 1$: the permeation law is no more isotropic. Similar observations

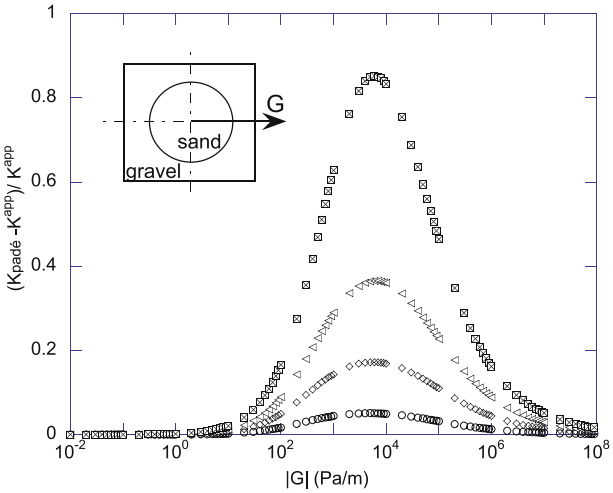

Fig. 7 Case 1: inclusions of sand embedded in a matrix of gravel. Relative error introduced by the Padé approximation versus the gradient of pressure for different volume fractions of inclusion. (○) $f = 0.1$, (◇) $f = 0.3$, (◁)$f = 0.5$, (☒) $f = 0.7$

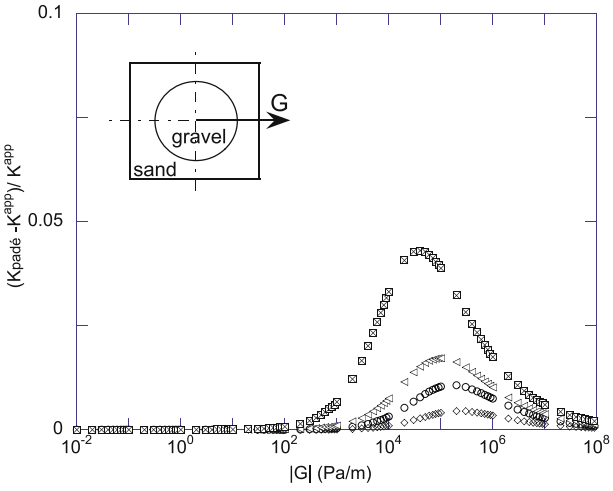

Fig. 8 Case 2: inclusions of gravel embedded in a matrix of sand. Relative error introduced by the Padé approximation versus the gradient of pressure for different volume fractions of inclusion. (○) $f = 0.1$, (◇) $f = 0.3$, (◁)$f = 0.5$, (☒) $f = 0.7$

were established in the case of flow of non-linear power law fluids though square arrays of parallel fibers of circular cross-section (Idris et al. 2004).

6 Conclusion

The modelling of high velocity flow in heterogeneous porous media has been investigated by upscaling the flow at the heterogeneity scale where the Forchheimer

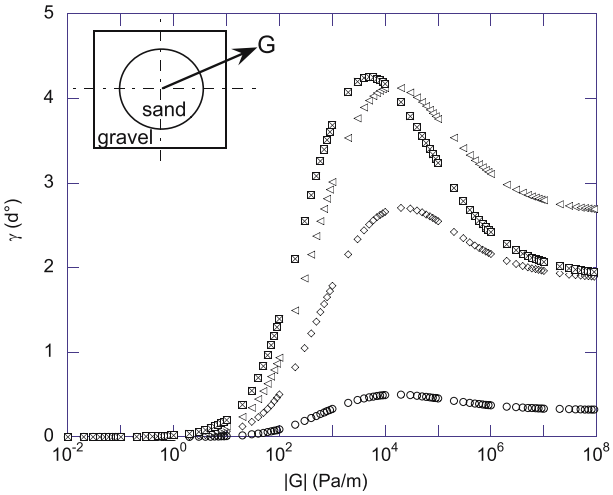

Fig. 9 Case 1: inclusions of sand embedded in a matrix of gravel. Evolution of the angle γ versus the gradient of pressure for different volume fractions of inclusion. ($\circ$)$f = 0.1$, ($\diamond$) $f = 0.3$, ($\triangleleft$) $f = 0.5$, ($\boxtimes$)$f = 0.7$

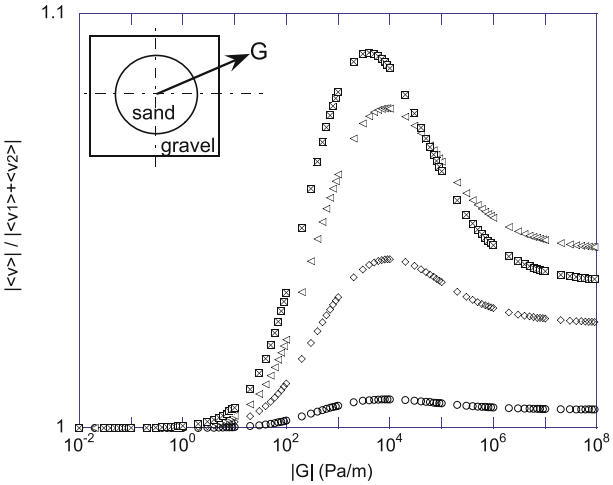

Fig. 10 Case 1: inclusions of sand embedded in a matrix of gravel. Relative error introduced by the Padé approximation versus the gradient of pressure for different volume fractions of inclusion. ($\circ$) $f = 0.1$, ($\diamond$) $f = 0.3$, ($\triangleleft$)$f = 0.5$, ($\boxtimes$) $f = 0.7$

law is assumed to be valid. We have first theoretically shown that Forchheimer law does not generally survive upscaling. It has also be shown that as Forchheimer law the macroscopic flow law is strongly non-linear, it is generally anisotropic for local geometries which yield isotropic Darcy law in the linear regime and it can not be satisfyingly described by a simple 2-point Padé–Forchheimer approximation, particularly in the case of inclusion more permeable than the matrix. Non-linearities reveal anisotropy in the macroscopic flow law directly connected with the geometry

anisotropy itself. Further work will concern the development of a methodology to formulate the macroscopic flow law.

References

Auriault, J.-L.: Heterogeneous medium. Is an equivalent macroscopic description possible? Int. J. Eng. Sci. **29**(7), 785–795 (1991)

Bensoussan, A., Lions, J.-L., Papanicolaou, G.: Asymptotic Analysis for Periodic Structures. North Holland (1978)

Bordier, C., Zimmer, D.: Drainage equations and non-Darcian modelling in coarse porous media or geosynthetic materials. J. Hydrol. **228**, 174–187 (2000)

Femlab: Reference Manual, version 3.1. http://www.consol.com

Firdaous, M., Guermond, J.L., Le Quéré, P.: Nonlinear corrections to Darcy's law at low Reynolds numbers. J. Fluid Mec. **343**, 331–350 (1997)

Forchheimer, P.: Wasserbewegung durch boden. Zeit Vereines Deutscher Ingnieure. **45**(49), 1736–1741 and (50), 1781–1788 (1901)

Fourar, M., Radilla, G., Lenormand, R., Moyne, C.: On the non-linear behavior of a laminar single-phase flow through two and three-dimensional porous media. Adv. Water Res. **27**, 669–677 (2004)

Fourar, M., Lenormand, R., Karimi-Fard, M., Horne, R.: Inertia effects in high-rate flow through heterogeneous porous media. Trans. Porous Med. **60**, 353–370 (2005)

Idris, Z., Orgéas, L., Geindreau, C., Bloch, J.-F., Auriault, J.-L.: Micromechanical effects on the flow law of power law fluids through fibrous media. Model. Simul. Mater. Sci. Eng. **12**, 995–1015 (2004)

Kanit, T., Forest, S., Galliet, I., Mounoury, V., Jeulin, D.: Determination of the size of the representative elementary volume element for ramdom composites: statistical en numerical approach. Int. J. Solids Struct. **40**, 3647–3679 (2003)

Kanit, T., N'Guyen, F., Forest, S., Jeulin, D., Reed, M., Singleton, S.: Apparent and effective physical properties of heterogeneous materials: representativity of samples of two materials from food industry. Comp. Meth. Appl. Mech. Eng. **195**, 3960-3982 (2006)

Marušić-Paloka, E., Mikelić, A.: The derivation of a nonlinear filtration law including the inertia effects via homogenization. Nonlinear Anal. **42**, 97–132 (2000)

Mei, C.C., Auriault, J.-L.: Mechanics of heterogeneous porous media with several spatial scales. Proc. R. Soc. Lond. A. **426**, 391–423 (1989)

Mei, C.C., Auriault, J.-L.: The effect of weak inertia on flow through a porous medium. J. Fluid Mech. **222**, 647–663 (1991)

Sanchez-Palencia, E.: Non Homogeneous Media and Vibration Theory. Lecture notes in Physics, vol. 127, Springer (1980)

Skjetne, E., Auriault, J.-L.: High-velcity laminar and turbulent flow in porous media. Trans. Porous Media **36**, 131–147 (1999)

Venkataraman, P., Rama Mohan Rao, P.: Darcian, transitional, and turbulent flow through porous media. J. Hydrol. Eng. **124**(8), 840–846 (1998)

Wodie, J.-C., Levy, T.: Correction non-linéaire de la loi de Darcy. C. R. Acad. Sci. Paris Ser II. **312**, 157–161 (1991)